Photo-double-ionization of Mg studied by electron-electron-coincidence experiments

E. Sokell,[1] P. Bolognesi,[2] A. Kheifets,[3] I. Bray,[4] S. Safgren,[1] and L. Avaldi[2]
[1]*School of Physics, UCD Science Centre, Belfield, Dublin 4, Ireland*
[2]*CNR-Istituto di Metodologie Inorganiche e dei Plasmi, Area della Ricerca di Roma1, 00015 Monterotondo Scalo, Italy*
[3]*RSPE, The Australian National University, Canberra ACT 0200, Australia*
[4]*ARC Centre for Matter-Antimatter Studies, Curtin University, WA 6845 Perth, Australia*
(Received 9 August 2013; revised manuscript received 9 November 2013; published 21 January 2014)

The photo-double-ionization (PDI) of Mg to the $Mg^{2+}(3s^{-2})$ state has been studied by photoelectron-photoelectron-coincidence experiments at a photon energy corresponding to the excitation of the $2p \rightarrow 3d$ resonance. The equal energy sharing ($E_1 = E_2 = 16.4$ eV) as well as the complementary unequal energy ($E_1 \leftrightarrow E_2 = 10.4 \leftrightarrow 22.4$ eV) sharing kinematics have been investigated. From the experimental results without any approximation the symmetrized gerade and ungerade amplitudes have been obtained. The experimental angular correlation patterns as well as the amplitudes are compared to CCC calculations in which the resonant process has been incorporated. The results confirm that the amplitudes of the photo-double-ionization carry the signature of the target radial wave function. The investigation of the triple differential cross sections has been then extended by simulations to a kinematics with the fixed detector at 90^o, which can not be studied experimentally by the present setup. These simulations shed light on results of previous measurements on alkaline-earth-metal atoms in this kinematics, which were not consistent with the common understanding of photo-double-ionization derived from He experiments.

DOI: 10.1103/PhysRevA.89.013413 PACS number(s): 32.80.Fb

I. INTRODUCTION

The study of emission of two electrons from an atom by absorption of a single energetic photon, a process referred to as atomic photo-double-ionization (PDI), has attracted a lot of interest because it provides unique information on the electron-electron interaction. Experiments in which either both the photoelectrons or one photoelectron and the recoil ion, after angle and energy selection, are detected in coincidence, provide the most detailed information on the process via the measurement of the triple differential cross section $d^3\sigma/dE_1 d\Omega_1 d\Omega_2$ (TDCS). For a long time, the study of PDI in the simplest two-electron system, the He atom, challenged both experimentalists and theorists and showed that the dynamics of the electron pair is strongly constrained by its own symmetry and the Coulomb repulsion. As far as the experiments on helium are concerned, different approaches to circumvent the low value of the double-ionization cross section have been devised and nowadays a broad set of data from threshold up to 450 eV above it in different energy sharing conditions of the electron pair are available [1]. On the theoretical side, PDI, which is the archetypal example of a three-body Coulomb problem, represents a nonseparable problem, and cannot be given an exact analytical solution. Methods in quantum mechanics have been developed to give nearly exact solutions for the He three-body ground and excited discrete states. However, the high doubly excited states and the double continuum states had to wait for the development of powerful computers to be accessible by numerical calculations. These methods have been reviewed first by Briggs and Schmidt [2] and, more recently, by Malegat [3]. The joint experimental and theoretical efforts have lead to a good understanding of the PDI process, at least as far as the two-electron He system is concerned.

Alkaline-earth-metal atoms (Be, Mg, Ca, Sr) are quasi-two-electron systems and represent the most suitable candidates for extending the investigation of PDI beyond He. In these atoms, the outer valence shell is well separated from the rest of the atom. Thus, in the PDI of the two outer shell electrons, the inner and subvalence electrons can be treated as spectators. With this assumption, the PDI process in alkaline-earth-metal atoms is similar to that in He except for a different radial structure of the target *ns* orbital and the influence of the distorting potential of the core on the departing photoelectrons. The theoretical photo-double-ionization cross section of Be and heavier alkaline-earth-metal atoms have been calculated within several theoretical schemes [4–10]. Recently Kheifets and Bray [11] made a systematic investigation of Be, Mg, and Ca to elucidate the role of both ground- and final-state correlations. Their results showed that the narrowing of the angular correlation is related to the shrinking of the *ns* orbital in momentum space. More recently [12] a strong effect of the target electronic structure was observed in calculations of the angular correlation pattern in the two-electron continuum following L-shell photo-double-ionization. It has been shown that (i) for a given symmetry of the electron pair the PDI angular correlation mimics the angular distribution of an electron impact ionization of the corresponding ion and (ii) the amplitudes of these processes are strongly determined by the radial extent and the oscillations of the target orbital of the singly charged ion.

On the experimental side, the ratio of the double to single photoionization cross sections, σ^{2+}/σ^{+}, of alkaline-earth-metal atoms has been measured for Be [13], Mg [14,15], Ca, and Sr [16]. Unfortunately, the low target density achievable in metal vapor beams exacerbates the low value of the PDI cross section. Thus, even at third-generation synchrotron radiation sources, the measurement of the TDCS is challenging and, to our knowledge, only a single TDCS in Ca has been reported in the nonresonant condition at an excess energy of 25 eV [17]. However, the presence of $np \rightarrow n'd$ resonances in the double continuum has made possible the measurement of the TDCS

in a few other cases [18–21]. While these resonances enhance the photoabsorption cross section and therefore the emission of the two electrons, they may affect the shape of the TDCS because the intermediate excited state populates the double continuum via the ejection of two electrons [22]. Indeed some anomalous observations in the TDCS of Ca and Sr measured at the $3p \rightarrow 3d$ and $4p \rightarrow 4d$ resonances, respectively, have been interpreted as a signature of this indirect process. These anomalies consisted of extra lobes in the TDCS with respect to the photo-double-ionization of He, in particular, when one electron is measured at 90° with respect to the polarization axis of the incident radiation.

In this work, we have measured the TDCS for the PDI of Mg at 55.49 eV, which corresponds to the excitation of the $2p \rightarrow 3d$ resonance, for equal energy sharing conditions ($E_1 = E_2 =$ 16.4 eV) and in two complementary unequal energy sharing conditions ($E_1 = 10.4$ eV, $E_2 = 22.4$ eV), where the kinetic energy of the photoelectrons $E_1 \leftrightarrow E_2$ has been exchanged. The TDCS has been also calculated by incorporating semiempirically the effect of the resonant excitation in the convergent close-coupling (CCC) [11] formalism. A subset of the data, taken in the equal energy sharing condition, has been recently presented in a Letter [23].

The paper is organized as follows, in Secs. II and III information about the experimental setup and procedures, and details of the theoretical model are presented. The experimental results and their comparison with the theoretical predictions are shown and discussed in Sec. IV. In the same section, we also address the specificity of the kinematics with a fixed electron measured at 90° with respect to the polarization axis of the incident radiation. Finally, conclusions are drawn in Sec. V.

II. EXPERIMENT

The experiments have been performed using the electron-electron multicoincidence end-station [24] at the Gas Phase Photoemission [25] beamline of the Elettra storage ring, where an undulator of period 12.5 cm, 4.5 m long, produces completely linearly polarized radiation in the photon energy range 13–1000 eV with a typical resolving power of 10000. In the present case, at the chosen photon energy, $h\nu = 55.49$ eV, the energy resolution was degraded to about 150 meV in order to increase the photon flux. The vacuum chamber hosts two independent turntables, holding respectively three and seven electrostatic hemispherical analyzers spaced by 30°. The three spectrometers of the smaller turntable are mounted at angles of 0°, 30°, and 60° with respect to the polarization vector of the light $\boldsymbol{e} = e\boldsymbol{x}$ and they have been used to measure the fixed electron, labeled 1, in the perpendicular plane. The larger turntable rotates in the plane perpendicular to the direction, z, of propagation of the incident radiation, and its seven analyzers have been used to measure the angular distribution of the correlated electron, labeled 2, of complementary energy in order to fulfill the energy balance $E_1 + E_2 = h\nu - I^{2+}$, where I^{2+} is the double-ionization potential. The ten analyzers have been set to detect electrons of kinetic energy $E_1 = E_2 = 16.4$ eV in the equal energy sharing experiment, and $E_1 = 10.4$ (22.4) eV, $E_2 = 22.4(10.4)$ eV in the two complementary unequal energy sharing experiments. The energy resolution and the angular acceptance in the dispersion plane of the spectrometers were $\Delta E/E_{1,2} = 0.03$ and $\Delta\theta_{1,2} = \pm 3°$, respectively. The relative angular efficiency of the ten analyzers has been established and checked by measuring the photoelectron angular distributions for photoionization of Mg $2p$ and Ne $2p$ electrons, with well-known asymmetry parameters, at the same excess energy above their respective ionization thresholds [26,27]. The same efficiency correction has been assumed for the coincidence measurements. The validity of this assumption was tested by measuring the coincidence yield at two positions of the larger turntable, which overlap the two analyzers nearby. Therefore, all the experimental data are cross normalized and can be reported on the same relative scale. This can be checked by observing that the same coincidence yield is measured for different configurations of the spectrometers, obtained by the interchange of energies and angles, which correspond to the same kinematics [28].

The metal vapor source is collinear with the photon beam, which passes through the hollow core of the source before interacting with the atomic beam. As described by Ross and West [29], two thin-walled stainless steel tubes are mounted on the base and the heater wires are held within these two tubes. The crucible, which holds the metal charge, is comprised of two coaxial cylinders, which are welded together at one end. A distinctive feature of this crucible is that it is possible to have any number of apertures drilled in the closure piece and pointing to the interaction region. The number of apertures used, six in the present experiments, thereby increases the atom density at the interaction region. Facing the oven a copper cylinder, coaxial with the photon beam and cooled to about 0 °C, traps the vapor beam, shielding the setup and preventing its contamination. Suitable holes on the two bases of the cylinder allow the photon beam to pass through, ending up on the photodiode, where its intensity is monitored throughout the experiments. This cylinder provides a relatively closed interaction region and openings on the lateral surface of the cylinder, three 1 cm holes for the fixed analyzers and a large slot of 230° for the rotatable analyzers, allow the photoelectrons to leave the interaction region to be detected. In addition, an independent hypodermic needle is allowed in the interaction region, pointing about 2 cm away from the vapor beam to prevent blockage, and is used to admit rare gases in the interaction region for tuning and calibration purposes. The oven has been operated with a temperature setting of 410 °C and 470 °C for the bottom and top parts of the crucible, respectively. An accumulation time of about three hours per point was necessary to reach the present accuracy in the experimental results.

III. THEORY

The CCC formalism as applied to alkaline-earth atoms has been described in Ref. [11]. In brief, the dipole matrix element of single photoionization leading to the final ionic state nl and continuum electron EL is obtained by the following integral

$$D_{nl\,El} = d_{nl\,EL} + \sum_{n'l'L'} \int_{E'} \frac{\langle nl\,EL \| T_{\mathcal{LS}} \| n'l'E'L' \rangle d_{n'l'E'L'}}{E + \epsilon_{nl} - E' - \epsilon_{n'l'} + i\delta}. \quad (1)$$

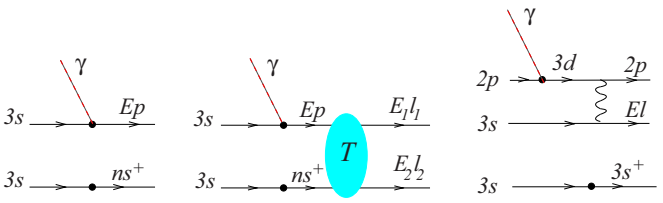

FIG. 1. (Color online) Diagrammatic representation of the direct (left) and resonant (right) single photoionization processes in the valence $3s^2$ shell of Mg. The horizontal lines visualize electrons, the dashed line represents the photon and the wavy line exhibits the Coulomb interaction. The central diagram exhibits the final-state correlation leading to doubly ionized continuum. The shaded oval represents the T matrix.

Here the bare dipole matrix element $d_{3s,Ep}$ for the case of Mg is visualized by the left diagram in Fig. 1. The final-state correlation is accounted for by integration of the bare dipole matrix element with half-on-shell T matrix in the dipole $\mathcal{L} = 1$ and singlet $\mathcal{S} = 0$ scattering state. The T matrix is found by solving a set of the integral Lippmann-Schwinger equations [30]. This correlation process is illustrated graphically by the central diagram of Fig. 1.

The dipole matrix element of single photoionization, Eq. (1), is used to construct the matrix element of PDI which corresponds to ejection of the photoelectron pair with the angular momenta l_1, l_2 and energies E_1, E_2:

$$D_{l_1 l_2}(E_1,E_2) = (-i)^{l_1+l_2} e^{i[\sigma_{l_1}(Z=2)+\sigma_{l_2}(Z=1)]} \times D_{n_1 l_1 E_2 l_2}\langle l_1 E_1 \| n_1 l_1\rangle. \quad (2)$$

Here $\langle l_1 E_1 \| n_1 l_1\rangle$ is the radial projection of the final ionized state on to the positive energy target state $n_1 l_1$ of the matching energy $\varepsilon_{n_1 l_1} = k_1^2/2$. The Coulomb scattering phases $\sigma_{l_2}(Z = 1)$ and $\sigma_{l_1}(Z = 2)$ are calculated using the asymptotic charge of the singly and doubly charged ions, respectively. The PDI matrix elements, Eq. (2), are then fed to the following expression for the TDCS, which takes the form of the partial wave expansion:

$$\frac{d^3\sigma}{d\Omega_1 d\Omega_2 dE_2} = \frac{8\pi^2\omega}{3c}\left|\sum_{l_1 l_2} \boldsymbol{e}\cdot Y_1^{l_1 l_2}(\boldsymbol{n}_1,\boldsymbol{n}_2) D_{l_1 l_2}(E_1,E_2)\right|^2. \quad (3)$$

Here $c \approx 137$ is the speed of light in atomic units. The unit vectors $\boldsymbol{n}_i = \boldsymbol{k}_i/k_i, i = 1,2$ are directed along the photoelectron momenta, $\boldsymbol{e}$ is the polarization vector of light. The bipolar harmonics $Y_1^{l_1 l_2}(\boldsymbol{n}_1,\boldsymbol{n}_2)$ are tensors of rank 1 [31].

The two-electron CCC formalism cannot tackle resonant processes *ab initio*. This process is exhibited by the right diagram of Fig. 1. In the nonresonant PDI process from the valence $3s^2$ shell of Mg, the role of the $2p \to \boldsymbol{\varepsilon} d$ transition was found insignificant as was confirmed by calculating single photoionization cross sections by the CCC and RPA methods, the latter with the full account of the intershell $3s^2$ and $2p^6$ correlation [11]. On the other hand, the resonant process lies at the heart of the resonant TDCS measurement, so it should be incorporated into the CCC formalism semiempirically. In doing so, we note that the dipole matrix element varies near the resonance as [32]

$$D(\omega) = \frac{q+\varepsilon}{i+\varepsilon} D_0 \cong -iq D_0 \quad (4)$$

at $\omega \approx \omega_0$ and $\varepsilon \approx \varepsilon_0$. Here $\varepsilon = (\omega - \omega_0)/(\Gamma/2)$ is the photon energy measured from the resonance in units of its width Γ, q is the profile (Fano) index and D_0 is the matrix element in the absence of the resonance. Equation (4) leads to the Fano formula for the cross section [33]

$$\sigma(\omega) = \frac{(q+\varepsilon)^2}{1+\varepsilon^2}\sigma_0 \cong q^2\sigma_0. \quad (5)$$

To incorporate the Fano formulae (4) and (5) into the CCC formalism, we modify the bare matrix element of single photoionization

$$d_{ns\ Ep} = \begin{cases} -iq\langle 3s\|r\|E_0 p\rangle\langle 3s\|ns^+\rangle & n=3, E_0 = \omega_0 + \varepsilon_{3s} \\ \langle 3s\|r\|E_0 p\rangle\langle 3s\|ns^+\rangle & \text{elsewhere} \end{cases}. \quad (6)$$

Here the profile index $q \approx -50$ for the resonant $2p \to 3d$ photoionization leaving the Mg^+ ion in its ground state [34] has been used. In principle, the resonance will be present in all energetically accessible final ns^+ channels, not only in the lowest $3s^+$ ionic state. However, each channel will have its own profile index, which is not known from experiment and is hard to calculate *ab initio*. So we ignore these resonances except in the ground ionic state, which makes the strongest contribution.

IV. RESULTS AND DISCUSSION

A. Results

The experimental results, as well as the CCC calculations with and without the inclusion of the resonance contributions in the case of the equal energy sharing ($E_1 = E_2 = 16.4$ eV) kinematics are shown in Fig. 2 for three fixed reference angles $\theta_1 = 0°$, 30°, and 60°. For the sake of comparison, the two calculations are normalized to each other to their maximum values in each figure. The absolute cross section is about a factor of four lower than in the calculations including the resonance (divided by the q^2 factor). The comparison between nonresonant and resonant CCC calculations shows that resonance does not introduce extra features in the TDCS, apart from the minor ones on the sides of the main peaks, but does change the relative intensity of the lobes.

At all θ_1, the TDCS shape displays a node at $\theta_{12} = 180°$ as expected for the singlet odd character of the double continuum wave function. At $\theta_1 = 0°$, the theory predicts two lobes of equal intensities while at $\theta_1 = 30°$ and 60° the TDCS is mainly concentrated in one structure with some minor features: a small lobe at about 230° and a nonvanishing cross section at about 100° at $\theta_1 = 30°$, a series of three small lobes at $\theta_1 = 60°$. The quality of the data does not allow the complete resolution of all of these features, but the general trend is in fair agreement with the predictions. At all θ_1, the additional feature predicted in the main lobe by the resonant CCC calculations, cannot be discerned in the experimental data. As far as the comparison with the double ionization of He for equal energy sharing at similar excess energy [35,23] is concerned, one sees that the

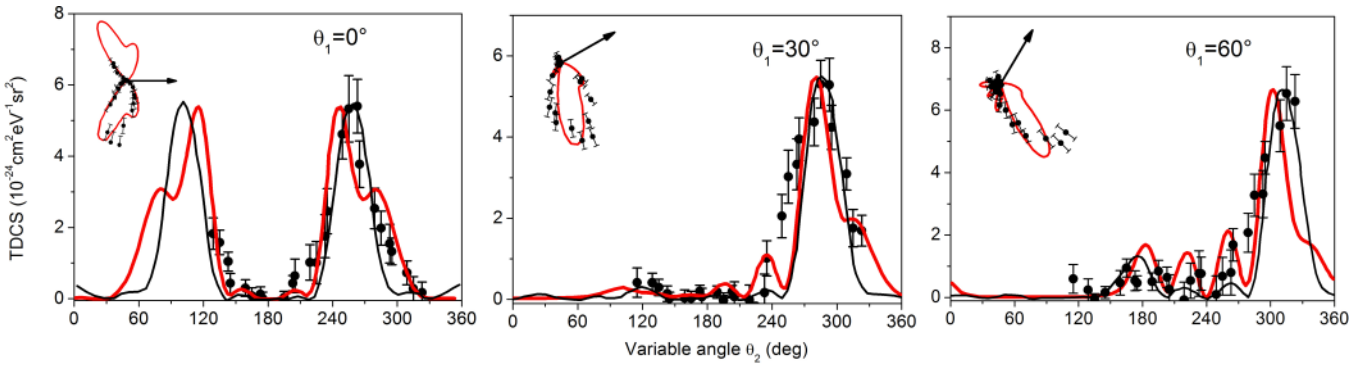

FIG. 2. (Color online) TDCS of Mg in equal energy sharing ($E_1 = E_2 = 16.4$ eV) kinematics for three fixed reference angles $\theta_1 = 0°$, 30°, and 60°compared with the resonant (red solid line) and nonresonant (black dashed line) CCC calculation. The experimental TDCS (shown with error bars) have been rescaled to the CCC calculations, which include the resonance process (see text). In the insets the polar plots of the TDCS are shown.

Mg TDCS share with He the node at $\theta_{12} = 180°$, but the lobes in Mg are significantly narrower and the relative intensity and number of minor lobes at $\theta_1 = 30°$ and 60° are different.

As the three TDCS were measured simultaneously, they can be reported on the same relative scale of intensity. A common scaling factor between theory and experiment has been used for the TDCS of Mg at $\theta_1 = 30°$ and 60°, while the theory appears to overestimate the experiment by a factor 2.2 at $\theta_1 = 0°$. Similar variation of the scaling coefficients by a factor of 1.6 was required for He [23], which indicates the level of agreement between the present theory and experiment that we may expect.

The experimental results for the unequal energy sharing kinematics $E_1 = 10.4$ eV and $E_2 = 22.4$ eV and the complementary kinematics where E_1 and E_2 are exchanged, as well as the corresponding resonant CCC calculations are shown in Figs. 3(a) and 3(b), respectively, for the fixed reference angles $\theta_1 = 0°$ and 30°. A common scaling factor between theory and experiment has been used for all these plots. In both kinematics, the theoretical TDCS at $\theta_1 = 0°$ are formed by three main lobes, with a peak at $\theta_2 = 180°$, because the back-to-back emission is no longer forbidden in the case of electrons of different energy, and two side lobes characterized by a double structure. The TDCS at $\theta_1 = 30°$

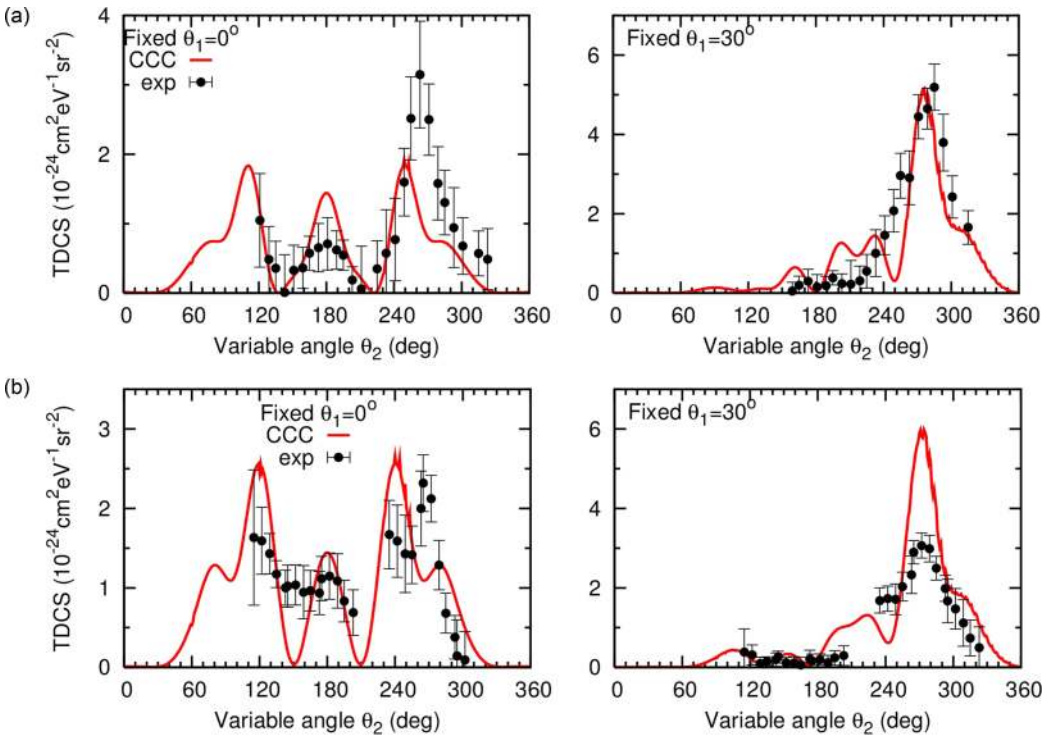

FIG. 3. (Color online) (a) TDCS of Mg in unequal energy sharing ($E_1 = 10.4$ eV, $E_2 = 22.4$ eV) kinematics for two fixed reference angles $\theta_1 = 0$ and 30°. The experimental TDCS (shown with error bars) have been rescaled to CCC (red solid line) (see text). (b) TDCS of Mg in unequal energy sharing ($E_1 = 22.4$ eV, $E_2 = 10.4$ eV) kinematics for two fixed reference angles $\theta_1 = 0°$ and 30°. The experimental TDCS (shown with error bars) have been rescaled to CCC (red solid line) (see text).

display a main feature and a series of minor lobes. The absolute value of the TDCS increases when θ_1 varies from 0° to 30° in both the complementary kinematics, and the TDCS in the two side lobes at $\theta_1 = 0°$ is smaller by a factor of 15–20% when the electron measured at a fixed angle is the slow one. The experimental results are quite consistent with the predictions, the main discrepancies being in the relative intensity of the side lobes at $E_1 = 10.4$ eV and $\theta_1 = 0°$, a shift of about 20° in the side peak at $\theta_1 = 0°$ in both complementary kinematics and the relative intensity of the different features at $E_1 = 22.4$ eV and $\theta_1 = 30°$, where theory overestimates by a factor of about 2 the feature at $\theta_2 = 270°$.

B. Discussion

As shown in a very general way by Briggs and Schmidt [2] by considering the invariance with respect to the rotation around the polarization direction of the incident radiation and the general properties of the spherical harmonics, the TDCS can be written in a way that allows full separation of the geometrical factors and the dynamical parameters. This leads to a parametrization of the TDCS, which is particularly useful because it can be easily linked to the experimental observations. In the case of incident radiation that propagates along the z axis and is fully linearly polarized along the $\boldsymbol{e} = e\boldsymbol{x}$ axis, the TDCS can be written as

$$\mathrm{TDCS}(E_1,E_2,\theta_{12}) \propto |a_g(E_1,E_2,\theta_{12})(\cos\theta_1 + \cos\theta_2) + a_u(E_1,E_2,\theta_{12})(\cos\theta_1 - \cos\theta_2)|^2, \quad (7)$$

where θ_{12} is the mutual angle of the two photoelectrons. The complex amplitudes a_g and a_u are respectively symmetric and antisymmetric in the exchange of E_1 and E_2. The θ_{12} and E dependence of these amplitudes includes all the physical information on the dynamics of the process, i.e., the effects of the electron-electron and electron-residual ion interactions.

In the case of equal energy sharing $a_u = 0$. Therefore the TDCS is fully determined by the symmetric, or gerade, amplitude

$$\mathrm{TDCS}(E_1,E_2,\theta_{12}) \propto |a_g(E_1,E_2,\theta_{12})(\cos\theta_1 + \cos\theta_2)|^2, \quad (8)$$

while in the case of unequal energy sharing, both the gerade and ungerade amplitudes contribute to the measured TDCS. Bolognesi *et al.* [36] proposed a procedure that allows the extraction of the moduli and relative phase of the a_g and a_u complex amplitudes from the experimental data. The method, which does not rely on any approximation, such as the Gaussian parametrization used for equal energy sharing in the case of He, needs only three determinations of the TDCS at the same relative angle θ_{12} between the photoelectrons and can be applied to any set of experimental data. The method, when applied to measurements with linearly polarized incident radiation, leaves undetermined the sign of the relative phase between the gerade and ungerade complex amplitudes [36]. The sign of the phase can be determined combining two sets of measurements with linearly and circularly polarized radiation [37].

The complex amplitudes have been extracted from the data either directly via Eq. (8) for the case of the equal energy sharing experiments or by applying the method developed by Bolognesi *et al.* [36] for the unequal energy sharing experiments. Having four determinations of the TDCS [the two complementary cases differ only by the sign in front

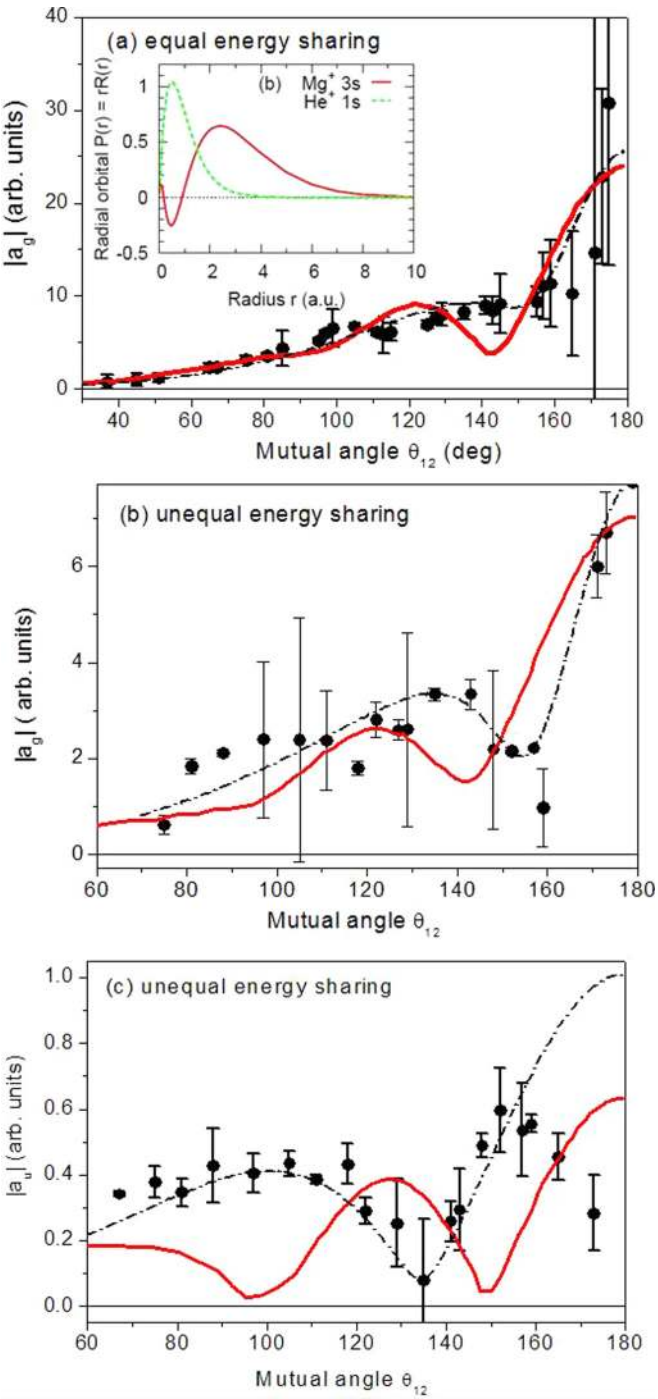

FIG. 4. (Color online) The symmetric gerade (a) amplitude for the equal energy sharing ($E_1 = E_2 = 16.4$ eV) kinematics and the gerade (b) and ungerade (c) amplitudes for the unequal energy sharing ($E_1 = 10.4$ eV, $E_2 = 22.4$ eV) kinematics. The resonant CCC calculations are represented by the red solid line in all figures. In Fig. 4(c) the CCC calculations have been rescaled to the experiments. The dashed black lines are the fits to the experimental amplitude with the di-Gaussian function Eq. (9). In the inset of panel (a) the radial orbitals $P(r) = rR(r)$ for Mg^+ $3s$ (red solid line) and He^+ $1s$ (green dashed line) are shown.

of the second addendum in Eq. (7)] the method proposed by Bolognesi *et al.* [36] can be applied to four different combinations of the measurements. To check the consistency of the results, the method has been applied to the different combinations and the results averaged. The experimental amplitudes are shown in Fig. 4, where also the predictions by CCC are reported.

The comparison between the CCC-calculated and experimental amplitudes is quite satisfactory in the case of the symmetric gerade amplitude for both the equal [Fig. 4(a)] and unequal [Fig. 4(b)] energy sharing, although the quality of the data hampers a clear observation of the predicted minimum in the amplitude for the equal energy sharing case. The ungerade amplitude is predicted to be about two orders of magnitude smaller than the gerade one,while in the experiment a factor of about fifteen has been found. In Fig. 4(c) the theoretical predictions have been rescaled to the experimental results. The shape of the experimental a_u displays a minimum shifted of about 20° with respect to the theoretical one. Considering the absolute values of the two amplitudes and the quality of the present measurements, the ungerade amplitude in the present kinematics might be too small to be reliably determined experimentally. However, the differences in the calculated and experimentally derived amplitude may also explain the differences observed in the TDCS (Fig. 3). The small value of the ungerade amplitude also explains why the shapes of the complementary kinematics are not too different. The relative phase between the gerade and ungerade amplitudes is approximately constant near $\theta_{12} = 180°$ with a value of $35 \pm 10°$. These findings are consistent with the ones in He. Indeed the analysis of the symmetrized amplitudes reported by Kheifets and Bray [38] at a few excess energies from 9–60 eV and several energy sharing ratios $R = E_1/E_2$ showed that, for example, at an excess energy of 40 eV and $R = 2.2$ the a_u/a_g ratio is about 0.1 and the contribution of the a_u amplitude becomes significant only at high excess energy and large R, where it explains the measured TDCS at $\theta_{12} = 180°$.

It is worth noting that all the calculated amplitudes in Fig. 4 display a similar shape with a main peak centered at the mutual angle $\theta_{12} = 180°$, a minimum whose relative intensity changes depending on the energy sharing and the gerade or ungerade symmetry and a secondary maximum at about $\theta_{12} = 130°$. This shape is far from the Gaussian shape proposed for the symmetric a_g amplitude in the equal energy sharing by Wannier-type theories [39] and found to be a useful approximation to describe He results up to an excess energy of 80 eV [38]. Recently, it has been shown that the a_g amplitude for the equal energy sharing case in the L-shell photo-double-ionization is better represented by a di-Gaussian parametrization [12]

$$a_g = G(A_1,\gamma_1,\theta_{12}) + e^{i\phi}G(A_2,\gamma_2,\theta_{12}), \tag{9}$$

where

$$G(A,\gamma,\theta_{12}) = A\exp[-2\ln 2(\theta_{12} - 180)^2/\gamma^2]. \tag{10}$$

The complex phase factor ϕ represents the interference of the two Gaussians. As was argued in Ref. [12], the Gaussian width may be linked to the radial extent of the target orbital of the singly charged ion. A sparser target orbital can be reached by a larger number of partial waves of the electron in the continuum, which leads to a narrower Gaussian. Thus, it is natural to associate the wide and narrow Gaussians with two characteristic regions in the target coordinate space. In PDI of the $2s$-shell atomic targets, these two regions are related to the positive and negative oscillations of the target orbital. In the present case of a $3s$-shell target orbital, there are three oscillations but the first one, near the origin, is very small as seen in the inset of Fig. 4(a) and hence will have a negligible contribution to the PDI amplitude.

The di-Gaussian function, Eq. (9), has been fitted to the experimentally determined amplitudes and the calculated ones. The five constants $A_{1,2}$, $\gamma_{1,2}$, and ϕ are used as fitting parameters. The obtained parameters are reported in Table I.

In the case of the equal energy sharing kinematics, the comparison between the theoretical and experimental di-Gaussian parameters is quite satisfactory [23]. The theoretical Gaussian width for He in similar kinematic conditions is 97°, which is close to the γ_2 parameter for Mg. This is consistent with the similar peak positions of the negative oscillation of the Mg^+ $3s$ orbital and the positive oscillation of the He^+ $1s$ orbital, as shown in the inset of Fig. 4(a). Even though the broader Gaussian peak is smaller than the central Gaussian peak, its contribution to the equal energy sharing TDCS is actually dominant. This can be easily understood because the Gaussian peak at $\theta_{12} = 180°$, which corresponds to the back-to-back emission, is suppressed by the kinematic factor due to the dipole selection rules, while the contribution of the broader Gaussian peak away from the kinematic node is not dampened.

Figures 4(b) and 4(c) show that both the experimental amplitudes in the unequal energy sharing experiments are well represented by a di-Gaussian function, although the poor quality of the data in the case of the ungerade amplitude results in a large uncertainty of the parameters. The fact that both amplitudes are well represented by the di-Gaussian function clearly indicates that they carry the signature of the

TABLE I. The parameters of the di-Gaussian function obtained by a fit to the present experimental data and the CCC calculations.

	Equal energy sharing		Unequal energy sharing			
	$E_1 = E_2 = 16.4$ eV		gerade amplitude		ungerade amplitude	
	Expt.	CCC [23]	Expt.	CCC	Expt.	CCC
A_2/A_1	0.42 ± 0.08	0.43	0.42 ± 0.03	0.53	0.54 ± 1	0.6
γ_1	$30 \pm 2°$	41.2	$28.5 \pm 1.5°$	42	$58 \pm 20°$	42
γ_2	$95 \pm 4°$	89.2	$96.2 \pm 2°$	75	$108 \pm 40°$	85
ϕ	$133 \pm 5°$	160	$153 \pm 3°$	165	$175 \pm 15°$	175

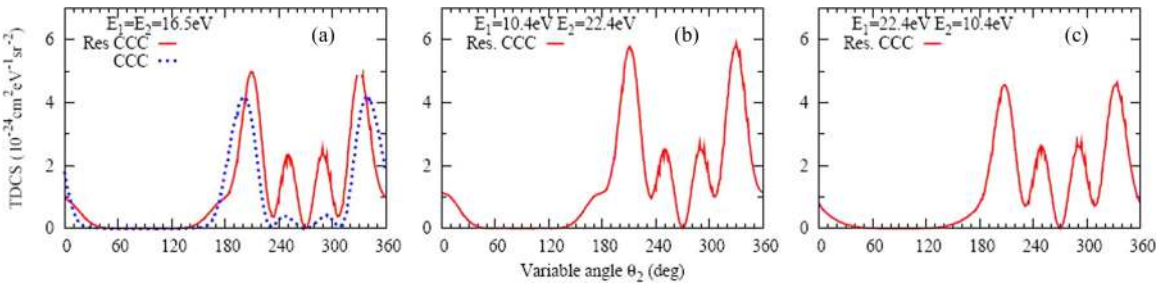

FIG. 5. (Color online) (a) The TDCS for the equal energy sharing condition at $\theta_1 = 90°$ calculated by CCC with (solid red line) and without (dotted blue line) the inclusion of the resonance effect. (b) The TDCS in an unequal energy sharing condition ($E_1 = 10.4$ eV, $E_2 = 22.4$ eV) and $\theta_1 = 90°$ calculated by CCC. (c) Same as in (b) but $E_1 = 22.4$ eV and $E_2 = 10.4$ eV.

singly charged ion orbital. However the relative contribution of the different regions in the coordinate space of the orbital is different in the two amplitudes. In the a_g amplitude the contribution of the large r region dominates, with the peak at $\theta_{12} = 180°$, while in the a_u one the contributions from the two regions are comparable. The experiments appear to give more relevance to the small r region with a broad feature with a maximum at $\theta_{12} = 110°$ than the theory.

C. TDCS with $\theta_1 = 90°$

The previous measurements of PDI in alkaline-earth-metal atoms have shown that the most intriguing results are obtained when the fixed electron is detected at $\theta_1 = 90°$ with respect to the direction of the polarization of the incident radiation in both equal and unequal energy sharing conditions. In the case of Ca, the TDCS measured by Ross *et al.* [18] in the region of the Ca $3p \rightarrow 3d$ resonances displayed two pairs of lobes in both the equal and unequal energy sharing kinematics. This is in contrast with the single pair observed in the TDCS of He. In the case of Sr, the TDCS measured by West *et al.* [20] and Sheridan *et al.*[21] in the region of the $4p \rightarrow 4d$ resonance showed a nonzero value for antiparallel ejection of the two electrons ($\theta_{12} = 180°$). This particular kinematics cannot be accessed with our present setup, thus we have performed here a simulation and analysis of the TDCS that can be expected on the grounds of the experimental and theoretical results presented in the previous sections.

First of all, the theoretical predictions for the equal energy sharing case [Fig. 5(a)] clearly show that the TDCS at $\theta_1 = 90°$ displays two pairs of lobes. A comparison between the two CCC calculations with and without the resonance effect proves that the effect of the resonance is to enhance the inner lobes, but the number of lobes is due to the initial-state wave function. A four-lobe structure is also predicted for the unequal energy sharing conditions [Figs. 5(b) and 5(c)] where the small value of the a_u amplitude makes the complementary TDCS very similar. These results are consistent with the observation of two pairs of lobes in the case of Ca [18] and clearly identify them as due to the target orbital wave function and not to an effect of the resonance.

In order to more accurately simulate the experimental TDCS, the experimental finite angular acceptance for each analyzer must be considered. Figure 6(a) shows the convolution of the theoretical TDCS at $\theta_1 = 90°$ with several θ_1 acceptances in the range $0° < \text{FWHM} < 20°$. This TDCS is represented by the di-Gaussian formula and the parameters listed in Table 1. An evolution of the shape of the TDCS is observed and a filling of the node at $\theta_{12} = 180°$ can be noticed. No significant changes in the shape of the TDCS were observed when $\theta_1 = 0°$.

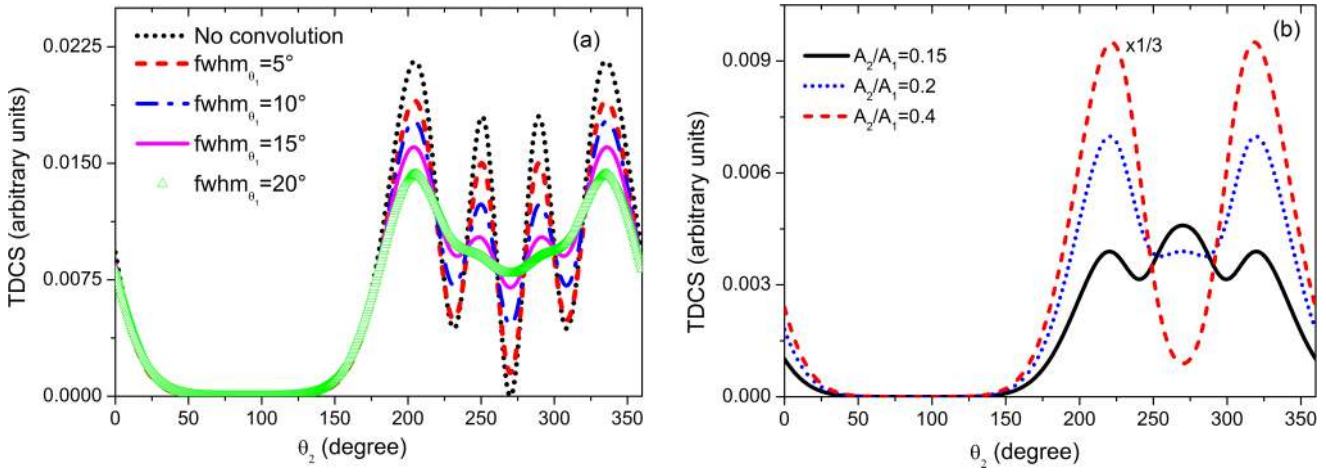

FIG. 6. (Color online) (a) Convolution of the TDCS at $\theta_1 = 90°$, calculated using the parameters from the fit to the CCC calculations (see text), by the angular acceptances θ_1 of the fixed electron. (b) Simulation of the TDCS at $E_1 = E_2 = 8$ eV with $\gamma_1 = 20°$, $\gamma_2 = 85°$, $\phi = 160°$, and FWHM $= 15°$ in θ_1 for three values of the A_2/A_1 ratio.

Furthermore, the inclusion of a finite θ_2 acceptance produces no appreciable changes in the shape of either of the simulated TDCS for $\theta_1 = 0°$ or 90°.

Figure 6(a) clearly illustrates that the TDCS measured at $\theta_1 = 90°$ can suffer from instrumental effects, which may mask or alter the real shape of the TDCS. However, even for a relatively large angular acceptance of 20^o, the TDCS has a minimum at $\theta_{12} = 180°$, in contrast to the local maximum generally observed experimentally in Sr [20,21].

Now, under the approximation that a di-Gaussian parametrization can be used also in the case of the photo-double-ionization of Sr to Sr^{2+} ($5s^{-2}$) state, the TDCS for the equal energy sharing case at about 8 eV above threshold has been simulated. In this simulation, we have taken into account that the Gaussian function becomes narrower as the atomic number of the alkaline earth increases and the excess energy decreases [11]. The calculated TDCS with $\gamma_1 = 20°$, $\gamma_2 = 85°$, $\phi = 160°$ and FWHM = 15° in θ_1 for several values of the A_2/A_1 ratio are shown in Fig. 6(b). The figure shows that there are conditions where a peak at $\theta_{12} = 180°$ appears in the TDCS.

The TDCS reported in Fig. 6(b) for $A_2/A_1 \leqslant 0.2$ might in principle explain the observation reported in the case of Sr [20,21]. However, the assumption of a di-Gaussian amplitude for the Sr gerade amplitude, the presumed A_2/A_1 ratio and the arbitrary parameters used for the convolution in θ_1, which are larger than the experimental ones [20,21], do not allow to definitely attribute the observed filling of the back to back node at $\theta_1 = 90°$ to instrumental effects. It is still possible that there is some violation of the symmetry selection rules. Nonetheless these findings set a claim for further measurements and calculations in this peculiar kinematics.

V. CONCLUSIONS

The TDCS of Mg at 55.49 eV have been measured in both equal ($E_1 = E_2 = 16.4$ eV) and complementary unequal energy ($E_1 \leftrightarrow E_2 = 10.4 \leftrightarrow 22.4$ eV) sharing kinematics. The basic quantities that determine the photo-double-ionization process, the symmetrized gerade and ungerade amplitudes and their relative phase, have been extracted from the experiment. The experimental results have been compared with CCC calculations, which incorporate the effect of the $2p \rightarrow 3d$ resonant excitation. The calculations show that the resonance enhances the absolute cross section and changes the relative intensity of some features, but it does not introduce extra features in the TDCS.

The main result is that both the complex amplitudes of the PDI process carry the signature of the singly charged ion orbital. This manifests in fringes of the amplitudes introduced by the radial oscillation of the target orbital. The observed shapes of the experimental amplitudes are well reproduced by the di-Gaussian parameterization, introduced for the equal energy sharing [12,23].

On the basis of the present findings, a simulation has been undertaken of the expected TDCS in equal energy sharing conditions when the fixed electron is detected at 90° with respect to the polarization of the incident radiation. In this kinematics two pairs of lobes are expected as observed in previous measurements on Ca and then a finite acceptance angle can lead to a TDCS with either a node or a peak at $\theta_{12} = 180°$. The first observation proves that the extra lobes observed in previous experiments are due to a target state effect and the observed changes in the relative intensity of the lobes are resonance dependent. The second observation provides a warning in the interpretation of a nonvanishing TDCS at $\theta_{12} = 180°$ in equal energy sharing experiments as a violation of the selection rules. Due to the approximations used in the simulation we cannot state that these results solve the previous puzzling observations in the TDCS of Sr, but provide a stimulus for future theoretical and experimental studies of PDI in alkaline-earth-metal atoms.

ACKNOWLEDGMENTS

Work partially supported by the MIUR PRIN 2009W2W4YF, 2009SLKFEX, and SFI Grant No. 08/RFP/PHY1117. The authors thank Paolo Bertoch and Federico Salvador for the prompt and qualified technical assistance in the assembling the Mg oven in the multicoincidence end-station of the Gas Phase Photoemission beamline at Elettra. Resources of the Australian National Computational Infrastructure Facility were used in this work.

[1] L. Avaldi and A. Huetz, J. Phys. B: At. Mol. Opt. Phys. **38**, S861 (2005).
[2] J. S. Briggs and V. Schmidt, J. Phys. B: At. Mol. Opt. Phys. **33**, R1 (2000).
[3] L. Malegat, Phys. Scr. T **110**, 83 (2004).
[4] A. S. Kheifets and I. Bray, Phys. Rev. A **65**, 012710 (2001).
[5] F. Citrini, L. Malegat, P. Selles, and A. K. Kazansky, Phys. Rev. A **67**, 042709 (2003).
[6] J. Colgan and M. S. Pindzola, Phys. Rev. A **65**, 022709 (2002).
[7] S. C. Ceraulo, R. M. Stehman, and R. S. Berry, Phys. Rev. A **49**, 1730 (1994).
[8] A. Kazansky and V. N. Ostrovsky, J. Phys. B: At. Mol. Opt. Phys. **30**, L835 (1997).
[9] F. Maulbetsch, I. L. Cooper, and A. S. Dickinson, J. Phys. B: At. Mol. Opt. Phys. **34**, L119 (2000).
[10] L. Malegat, F. Citrini, P. Selles, and P. Archirel, J. Phys. B: At. Mol. Opt. Phys. **33**, 2409 (2000).
[11] A. S. Kheifets and I. Bray, Phys. Rev. A **75**, 042703 (2007).
[12] A. S. Kheifets, I. Bray, J. Colgan, and M. S. Pindzola J. Phys. B: At. Mol. Opt. Phys. **44**, 011002 (2011).
[13] R. Wehlitz, D. Lukić, and J. B. Bluett, Phys. Rev. A **71**, 012707 (2005).
[14] R. Wehlitz, P. N. Juranić, and D. V. Lukić, Phys. Rev. A **78**, 033428 (2008).
[15] R. Wehlitz and P. N. Juranić, Phys. Rev. A **79**, 013410 (2009).
[16] E. Kayama *et al.*, J. Phys. Soc. Jpn. **75**, 044301 (2006).
[17] H.-J. Beyer, J. B. West, K. J. Ross, and A. De Fanis, J. Phys. B: At. Mol. Opt. Phys. **33**, L767 (2000).
[18] K. J. Ross, J. B. West, and H.-J. Beyer, J. Phys. B: At. Mol. Opt. Phys. **30**, L735 (1997).

[19] K. J. Ross, J. B. West, H.-J. Beyer, and A. De Fanis, J. Phys. B: At. Mol. Opt. Phys. **32**, 2927 (1999).
[20] J. B. West, K. J. Ross, H.-J. Beyer, A. De Fanis, and H. Hamdy, J. Phys. B: At. Mol. Opt. Phys. **34**, 4169 (2001).
[21] P. Sheridan, M. Grimm, and E. Sokell, J. Phys. B: At. Mol. Opt. Phys. **41**, 165204 (2008).
[22] M. Ya. Amusia, V. A. Kilin, A. Ehresmann, H. Schmoranzer, and K.-H. Schartner, J. Phys. B: At. Mol. Opt. Phys. **26**, 1281 (1993).
[23] E. Sokell, P. Bolognesi, A. Kheifets, I. Bray, S. Safgren, and L. Avaldi, Phys. Rev. Lett. **110**, 083001 (2013).
[24] P. Bolognesi *et al*., J. Electron. Spectrosc. Rel. Phenom. **141**,105 (2004).
[25] R. R. Blyth *et al*., J. Electron Spectr. Rel. Phenom. **101-103**, 959 (1999).
[26] S. H. Soutworth, A. C. Parr, J. E. Hardis, J. L. Dehmer, and D. M. P. Holland, Nucl. Instrum. Meth. A **246**, 782 (1986).
[27] B. Kämmerling, A. Hausmann, J. Laüger, and V. Schmidt, J. Phys. B: At. Mol. Opt. Phys. **25**, 4773 (1992).
[28] P. Bolognesi *et al*., J. Phys. B: At. Mol. Opt. Phys. **34**, 3193 (2001).
[29] K. J. Ross and J. West, Meas. Sci. Technol. **9**, 1236 (1998).
[30] D. V. Fursa and I. Bray, Phys. Rev. A **52**, 1279 (1995).
[31] D. A. Varshalovich, A. N. Moskalev, and V. K. Khersonskii, *Quantum Theory of Angular Momentum* (World Scientific, Philadelphia, 1988), 1st ed.
[32] M. Y. Amusia and A. S. Kheifets, Phys. Lett. A **82**, 407 (1981).
[33] U. Fano, Phys. Rev. **124**, 1866 (1961).
[34] M. Stener, G. De Alti, G. Fronzoni, and P. Decleva, Chem. Phys. **222**, 197 (1997).
[35] P. Bolognesi *et al*., Phys. Scr. T **110**, 62 (2004).
[36] P. Bolognesi, A. S. Kheifets, I. Bray, L. Malegat, P. Selles, A. K. Kazansky, and L. Avaldi, J. Phys. B: At. Mol. Opt. Phys. **36**, L241 (2003).
[37] P. Bolognesi, V. Feyer, A. Kheifets, S. Turchini, T. Prosperi, N. Zema, and L. Avaldi, J. Phys. B: At. Mol. Opt. Phys. **41**, 051003 (2008).
[38] A. S. Kheifets and I. Bray, Phys. Rev. A **65**, 022708 (2002).
[39] A. R. P. Rau, J. Phys. B **9**, L283 (1976); J. M. Feagin, J. Phys. B: At. Mol. Opt. Phys. **17**, 2433 (1984); J.-M. Rost, *ibid.* **27**, 5923 (1994).